World Academy of Science, Engineering and Technology
International Journal of Materials and Metallurgical Engineering
Vol:16, No:9, 2022

Microstructural Evolution of an Interface Region in a Nickel-Based Superalloy Joint Produced by Direct Energy Deposition

M. Ferguson, T. Konkova, I. Violatos

***Abstract*—**Microstructure analysis of additively manufactured (AM) materials is an important step in understanding the interrelationship between mechanical properties and materials performance. Literature on the effect of a laser-based AM process parameters on the microstructure in the substrate-deposit interface is limited. The interface region, the adjoining area of substrate and deposit, is characterized by the presence of the fusion zone (FZ) and heat affected zone (HAZ) experiencing rapid thermal gyrations resulting in thermal induced transformations. Inconel 718 was utilized as a work material for both the substrate and deposit. Three blocks of Inconel 718 material were deposited by Direct Energy Deposition (DED) using three different laser powers, 550W, 750W and 950W, respectively. A coupled thermo-mechanical transient approach was utilized to correlate temperature history to the evolution of microstructure. Thermal history of the deposition process was monitored with the thermocouples installed inside the substrate material. Interface region of the blocks were analysed with Optical Microscopy (OM) and Scanning Electron Microscopy (SEM) including electron back-scattered diffraction (EBSD) technique. Laser power was found to influence the dissolution of intermetallic precipitated phases in the substrate and grain growth in the interface region. Microstructure and thermal history data were utilized to draw conclusive comparisons between the investigated process parameters.

***Keywords*—**Additive manufacturing, direct energy deposition, electron back-scatter diffraction, finite element analysis, Inconel 718, microstructure, optical microscopy, scanning electron microscopy, substrate-deposit interface region.

I. Introduction

INCONEL 718 is a Ni-based superalloy designed to tolerate severe operating conditions that demand mechanical superiority in harsh service environments. Due to its excellent elevated temperature properties (up to 650 ºC) that include corrosion and oxidation resistance in combination with high creep and fatigue resistance, the superalloy is commonly used to manufacture aero-engine components and gas turbine disks [1]. The outstanding mechanical performance is due to the microstructure and precipitation kinetics formed during solid solution and subsequent heat treatments. AM capabilities have significantly evolved over the last few decades by optimizing process parameters for repair and remanufacturing abilities [2]. DED is an AM technique developed from powder injection laser cladding and rapid prototyping [3], [4]. A localized heat source generates a melt pool on the substrate surface, to which blown powder is directly fed relative to the raster though a nozzle with a carrier gas directly into the focal point of the laser During the build process, feedstock, either powder or wire, is fed directly into the molten pool created by the localized laser heat source which solidifies and successively creates a metallurgical bonded component [5].

The DED process can be used to manufacture components with complex geometries that require intricate manufacturing and to repair worn parts, such as turbine blades, and disks. Repairing gas turbine engine components reduces high manufacturing costs incurred during replacement parts while improving waste reduction.

The final microstructure is determined by the localised thermal history experienced during manufacturing [6]. By correlating process parameters to temperature history and utilizing these data to deduce microstructural features, the mechanical properties can be determined. Numerous studies have examined the microstructure of AM IN718 in as-deposited and post heat treatment conditions [7]-[13]. Most investigations predominately focus on the deposited component with the interface region receiving very little attention. The published literature mentions the interface as a band near the substrate/ deposit boundary, where the δ-phase had dissolved into the γ matrix [14]-[17]. The δ-phase is incoherent with the γ matrix and forms at grain boundaries, playing a key role in grain size control in wrought IN718 [18]. The interface region comprises of the joint layer where the parent material and deposit material are joined during DED. During the build process, this region is subjected to complex thermal gyrations, steep thermal gradients, and rapid cooling rates. When considering the thermal history experienced, the microstructural evolution response is vitally important for an outstanding metallurgical bond. The resultant complex thermal histories influence the microstructure, mechanical properties, and residual stresses in the final part.

To correlate the temperature history and resultant phenomena's, many researchers use the finite element analysis (FEA) to model the DED process and study the effects on the parts. However, existing data on temperature history are still

Ferguson, M. is from Design, Manufacturing & Engineering Management (DMEM) Department at the University of Strathclyde, Glasgow, G1 1XJ, (corresponding author, phone: +44141 534 5200; e-mail: matthew.ferguson@strath.ac.uk)

Konkova, T. is from DMEM Department at the University of Strathclyde, Glasgow, G1 1XJ, UK.

Violatos, I. is from Advanced Forming Research Centre (AFRC), University of Strathclyde, 85 Inchinnan Drive, Inchinnan, Renfrewshire, Scotland PA4 9LJ, UK.

limited [19]-[26].

The objective of this work is to develop a thermal model of the DED process and validate the predicted thermal response with in-situ temperature measurements. The experimentally validated thermal model will be utilized to deduce the evolution of microstructure in the interface of DED IN718, based on the simulated temperature history experienced.

II. Methodology

A. Experimental Procedure

A 2.5 kW continuous wave YAG fibre laser deposition system from nLIGHT® Alta™ which reproduced a 2 mm laser spot diameter at the substrate surface was used in the experiments. The configuration consists of a coaxial Hybrid™ AMBIT™ series mill head which is fitted to a Nikken rotary/tilt unit which allows 5-axis of deposition. Process parameters used in the experiments were chosen from literature review [8], [11], [14], [16], [27]-[30] and these can be seen in Table I. The coaxial nozzle with powder convergence point focused on deposition substrate surface was utilized. Argon was used as the carrier and shielding gas with a flow rate of 5 L min^{-1} and 8 L min^{-1}, respectively. The surface of the wrought IN718 substrate was polished by abrasive paper to remove oxide layer and cleaned with acetone before the DED process. Each sample consisted of a single clad track and an offset ten-layered solid block where each layer consisted of ten adjacent tracks deposited unidirectionally. A 50s dwell time was considered for the block to reach room temperature between single and block deposition. After the DED, samples were left at room temperature to cool.

TABLE I
PROCESS PARAMETERS USED FOR EXPERIMENTAL DEPOSITION

Laser Power (W)	Scanning Velocity (mm/s)	Powder feed rate (g/min)	Increment of Z axis (mm)	Overlap (%)
950	10	6	0.5	20
750	10	6	0.5	20
550	10	6	0.5	20

In this research, temperature measurements were performed using thermocouples of type-N with a 1.0 mm diameter. Nicotherm D™ Sheath has a measuring range from -270 ºC to 1250 ºC and were calibrated in-house using a Martel Electronics Precision Temp Calibrator. A total uncertainty of ± 2.4 ºC was found for temperature measurements. A total of 12 (*TC1-12*) 1.1 mm diameter holes were drilled via w-EDM to a distance of 23 ± 0.2 mm, leaving approximately 0.7 mm between deposited surface and thermocouple tip. The temperatures were recorded at the start, middle and end of the single track and repeated for solid blocks as cooling rates would differ depending on thermocouple location. Each thermocouple and corresponding hole were captured. A National Instrument CompactDAQ chassis was connected to a PC and recorded the temperatures in high resolution and high speed in Labview® at a rate of 50 Hz. Temperature measurements were recorded for the single clad track and solid block in each power case. The 950W experiment was repeated twice for validity. The thermocouples were inserted as functionally possible without damaging the flexible sheath and the depth of each thermocouple was measured post deposition.

An inverse heat transfer coefficient (HTC) experimental trial was carried out by placing the thermocouple equipment in a substrate, placed in a Carbolite® furnace, heated to set temperature followed by cooling via natural convection in air. The temperature history was collected.

After DED, samples were sectioned using w-EDM. The microstructure of both parallel section (X-Y plane) and transverse section (X-Z plane) were observed by OM using a Leica™ DM12000 and SEM equipped with electron back-scattered detection using an FEI Quanta™ 250 fitted with Oxford Instrument EBSD detector. Samples were prepared by standard technique grinding and polishing process which is finished by 0.02 µm colloidal silica suspension. For the OM, samples were etched using Kallings No.2 reagent with water.

B. Numerical Simulation

An experimentally validated numerical transient thermal finite-element (FE) simulation was conducted in the commercial welding MSC software Simufact Welding 8.0. The module incorporates a "quiet-element technique" to model powder addition. In general, a finer mesh will improve the accuracy of the calculation although at the penalty of computational time. A mesh sensitivity study was performed to optimize the convergence of accuracy and computational time. Considering that the interface region is subjected to the largest temperature gradients and most concentrated stresses, a refinement was used in this region with coarser mesh away from this region. All meshes were defined in ABAQUS® FE code imported to Simufact. In this simulation, the mesh was divided by linear brick elements (DC3D8), comprising of 179,039 mesh elements and 190518 mesh nodes. Temperature-dependent material properties based on [31], [32] were used to eliminate simulation error induced by mismatched physical properties at different temperatures.

A moving 3D double ellipsoidal heat source model developed by *Goldak* [33] simulated the heat input from laser deposition. Based on microstructural observations, the geometry of the melt pool including length, depth and width could be experimentally validated by the single track.

A power absorption efficiency of 0.37 [34] was used as a benchmark, requiring experimental calibration as discussed in Section III. Convective and radiative boundary conditions were applied to all free surfaces, including those of newly deposited material.

At the clamped boundaries, the substrate is in contact with metallic surroundings and the convective HTC was replaced with a contact HTC∝ with a value of 1200 W/(m^2.K) [24] to simulate strong heat loss from metallic clamp contact.

III. Calibration of Thermal Model

Fig. 1 shows the thermal history captured for different thermocouples in the substrate, which were compared to *'particle placements'* temperature history in Simufact welding 8.0. Simulations were calibrated by measuring the heat source

geometry using OM, performing an inverse simulation for the process efficiency, η, and calculating temperature-dependent convection coefficient values using inverse HTCs. The simulated temperature history for all 12 thermocouples is in close agreement with the experimental thermocouple measurements which capture similar peak temperatures and trends.

IV. Results and Discussion

A. Interface Investigation

The interface region between the as-deposited clad and substrate material revealed a white band as previously cited [14]-[16], [35] that, for 950W, ranged from 330 µm at the melt pool midpoint (maximum temperature) to 220 µm towards the edge of the melt pool due to the gaussian distribution. The bright band decreased in depth with decreasing laser power, the 750W had a maximum depth of 230 µm with 135 µm at the edge and the 550W had a maximum of 210 µm with 190 µm at the edge.

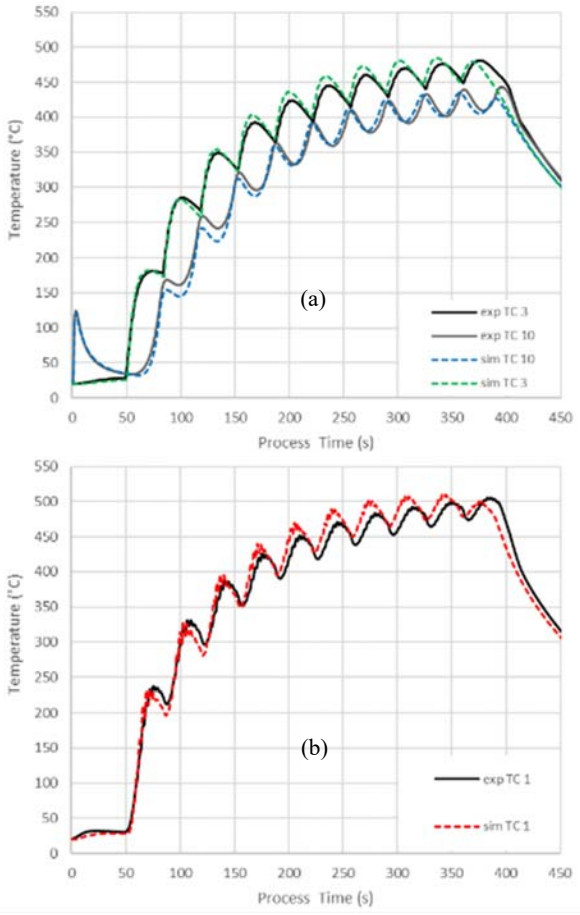

Fig. 1 Comparison between experimental data and simulated data for (a) TC10 (Single clad track) & TC3 (first TC at track 1 of solid block) and (b) TC 1 (final TC at track 10 of deposited block)

Fig. 2 shows a comparison between an optical micrograph capturing the cross-sectional (x-z) interface region (Track 6, P = 950W) and simulated thermal gradient for track 6. The interface region can be described as the clad zone (CZ), the partially melted zone (PMZ), the HAZ and the DA IN718 parent material (PM), which experience slightly different temperature histories.

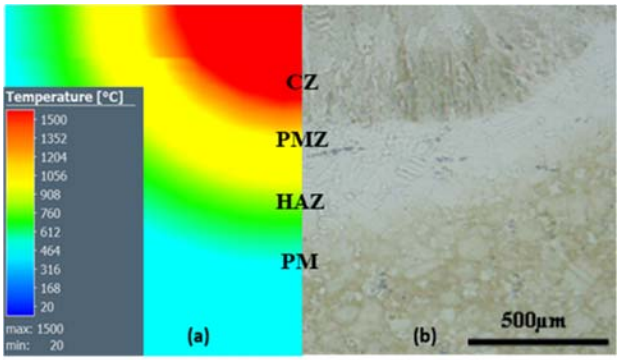

Fig. 2 (a) Thermal gradient for melt pool, P = 950W (b) Optical microscope of interface region as-deposited Inconel 718 superalloy

Analysing the bright band near the substrate/deposit interface, the PM equiaxed microstructure appeared less obvious (Fig. 2 (b)). In the PMZ region, there is strong evidence to support that the δ-phase was dissolved into the γ matrix. This dissolution of δ-phase (around 996-1015 °C [36]) would effectively 'unpin' the microstructure, which could result in grain growth and produce a higher Nb content in this region. If the as-deposited samples were subjected to an aging heat treatment, this could promote a higher density of strengthening phases dispersed across the interface region and thus improved strength [15]. Fig. 3 reveals the presence of solid solution carbides which were randomly dispersed throughout the substrate and remained across the PMZ due to their relatively high solvus temperature (around 1277 °C [37]). The microstructural features coupled with the data predicted by the thermal model (Fig. 4) collate this PMZ region experiences a temperature history between 996 °C and 1277 °C during the first layer of deposition. Both experimental and simulation data captured agree with previously published literature [14], [15].

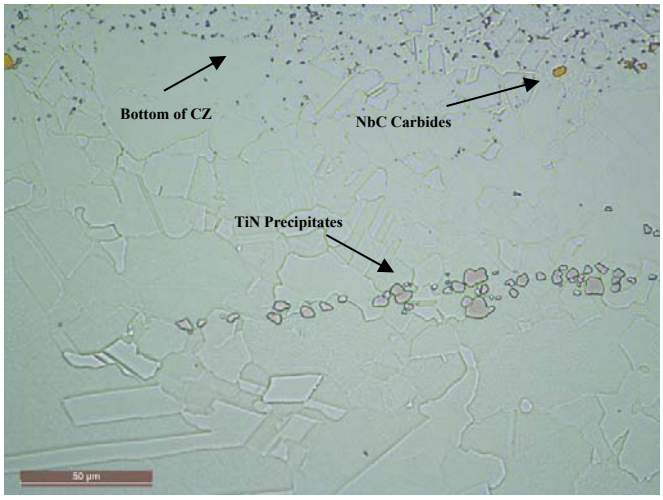

Fig. 3 Optical micrograph of Interface for P = 950W, detailing the presence of both NbC and TiN solid solution precipitates

The temperature history experienced at the PMZ was retrieved from the thermal models as shown in Fig. 4. This information will be vital to correspond evolution of microstructure and microstructural features. Due to the sluggishness of δ, Alloy 718 is thermo-mechanically stable up to around 650 °C, whereas key thermal induced phase changes occur above this temperature [38]. The 650 °C application limit is due to the conversion of γ'' to δ which is accelerated when thermal exposure is over 650 °C. At ~900°, δ takes preferential precipitation, so no precipitation of strengthening phases γ'' can occur. This preferential precipitation is up to ~1010 °C [39].

The role of Nb segregation on phase precipitation is largely influenced by the solidification sequence, but a heat treatment effect from laser attenuation will play a significant role in microstructural evolution.

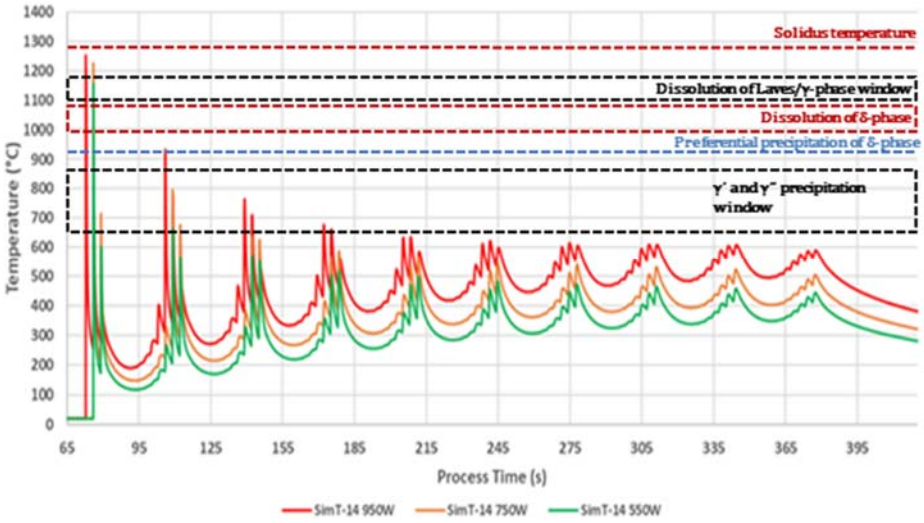

Fig. 4 HAZ temperature history retrieved from thermal model experienced for all three process parameter conditions

Although the presence of δ-phase will inhibit grain growth, the dissolution of δ phases back into the γ-matrix will produce a higher Nb density in that region and subsequent layer addition could replicate or initiate DA aging treatment, thus improving strength at the interface [15]. At temperatures 985 C, the δ-phase was seen to dissolve by almost 50pct, and was completely dissolved by 1010 C [14], [40]. In the higher temperature regions, the dissolving reaction of Laves/γ eutectic initiates around 1080-1140 C [41] and sufficient Laves phase is dissolved at 1150 C [42] (homogenization temperature) which could release more Nb content that could redistribute homogenously in the austenitic matrix. In addition to the alloying elements being dissolved back into the matrix, the Laves phase is well documented as detrimental to mechanical properties [15], [42], [43]. In Sui et al.'s study, it was determined that the failure mechanism of LMD IN718 was microscopic holes coalescence ductile fracture and that Laves phase was the main nucleases for microscopic hole formation [14].

Although standard homogenization of IN718 normally occurs for 1h and the DA requires a 2-step process for 8 hours each step, the temperature history for all three power cases in the PMZ region is sufficient for partial dissolution of δ-phase. Moreover, the subsequent layer deposition resulted in a heat treatment effect and a temperature retained close to the γ'/γ'' precipitation. Therefore, the microstructural response to temperature requires a more in-depth investigation.

V. Microstructural Evolution

In the cladding zone, it could be seen that columnar dendrites grew epitaxially along the deposition direction from the substrate zone (Fig. 2). This characteristic of directional solidification occurs when the heat loss direction during the solidification of the melt pool is about perpendicular to the surface of the substrate resulting in the epitaxial directional growth [14], [44]. The dendrite formation along the substrate interface is an outcome of the localized, instantaneous cooling rates occurred during solidification. Fig. 5 represents the cross-sectional microstructure of LMDed IN718, consisting of mainly austenitic matrix and continuous networks of Laves phase that occurs parallel to the build direction. As successive layers are added, the isotherm penetrates the surface of the previously deposited layer and remelts a region, the dendrites continue to grow along previous direction and form the combination of continuous and course Laves with strong directional selectivity [42]. The ultra-rapid cooling rate 10^3-10^6 C/s of laser metal deposition limits the network to mainly consist of primary dendrite arms located very close to one another, hindering the growth of secondary/tertiary arms. The epitaxial grown dendrites curve towards the heat source to ensure the maximum thermal gradients present at solid-liquid interface are maintained with proceeding growth [8].

The primary dendrite arm spacing of columnar dendrites at the interface were measured for Layer 1, Track 6 in all three power cases, using ImageJ analysis. These measurements are to quantitively compare microstructures and understand the cooling rates experienced from solidification, these results are

shown in Table II.

TABLE II
PRIMARY DENDRITE ARM SPACING MEASUREMENTS

Power	950W	750W	550W
Average PDAS (μm)	4.2	3.5	3.1
Standard deviation (μm)	0.87	0.72	0.64

The cooling rate is expected to increase with decreasing the laser power considering that coarser dendrites were given sufficient time to evolve during solidification. The highest cooling rate, based on the smallest PDAS will produce a very fine dendritic structure. A reason for this phenomenon occurring is due to the melt pool size. The 950W inputs more energy to the melt pool region, therefore creating a slightly larger melt pool than the other two process parameters. A slightly larger melt pool size will in effect take incrementally longer for all the material to reach solidification temperature given the ability to retain more thermal energy [43].

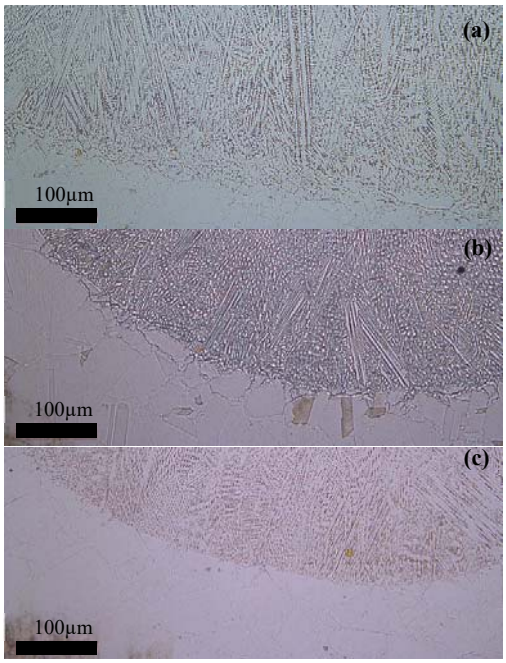

Fig. 5 Optical micrograph of cross section (x-z) for (a) P = 950W, (b) P = 750 and (c) P = 550W

Fig. 6 shows an SEM image of the cross-sectional morphology for the as-deposited clad layer in the P = 950W sample, specifically right at the interface region. The solidification sequence for as-deposited IN718 is well understood to be L→L + γ →L + Nb/γ → L + γ → Laves/γ [45]. And due to the low content of C present, formation of Nb carbides is negligible. Therefore, the dark grey phase in Fig. 6 can be identified as the austenite matrix γ phase and the dispersive white bright phase as interdendritic Laves phase, which have been identified using Energy Dispersive Spectrometer (EDS) and TEM in literature [9], [15]. The relatively thick and continuous networks of Laves phase were found in all three power cases. Due the high thermal gradient and instantaneous cooling rates experienced at the FZ; the fine columnar dendrite morphology is observed with interdendritic laves forming irregular shaped but continuous networks from the interface region. Brittle laves phase is detrimental to mechanical properties [46] with a wide-range-melting and precipitation temperature of 650 →1100 C, where temperature limits can vary with constituents. Homogenization is often employed to completely irradicate the brittle interdendritic phase as it depletes the γ matrix of Nb, a key element in the strengthening γ'' phase [7].

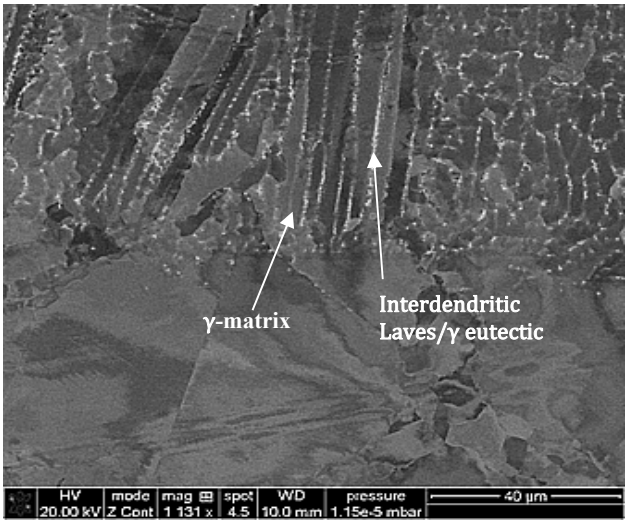

Fig. 6 Interface region P = 950W, showing Austenitic γ-matrix with interdendritic Laves/γ eutectic

During the DED process, most of the heat is dissipated through the substrate and previously deposited layers which both act as heat sinks. Heat flow direction can be explained using Fig. 7, the black arrows indicate directional solidification. During the solidification of the melt pool, heat flow direction is approximately perpendicular to the surface of pre-deposited layers and substrate. In this direction, the maximum thermal gradient is achieved, leading to the directional growth of dendrites grown from the bottom up. The directional solidification of the dendrites is explained with respect to maximum heat flux vector, Q [14]. Q_h represents the horizonal heat flux through previously deposited material due to deposition direction and Q_v is the heat flux through the wrought substrate. Heat loss is much lower in the horizontal direction than in vertical direction, therefore the resultant vector Q is approximately parallel to the build direction and grows epitaxially from the bottom up, aligned with the greatest thermal gradient, towards the scanning direction resulting from competitive growth of dendrites [9], [47]. This directional solidification would be in the tailing edge of the melt pool, the last section to solidify.

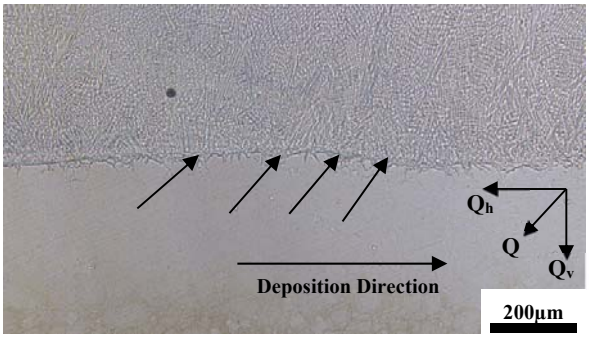

Fig. 7 Directional solidification, P = 750W

A. Grain Selection and Texture

Fig. 8 shows the inverse pole figure map generated from the EBSD analysis at the interface region of the 950W sample, with build direction along the growth direction (Y). Most grains grow in the direction of {100} family of grain planes with a preferential growth <001> for face-centred alloy IN718 [48]. Along the interface, depending on solidification conditions, nucleation or growth may be predominant. The melt pool centre consists of a region with maximum thermal gradient and grains with favourable <100> direction can grow epitaxially from the PM, parallel to heat flow direction. As the laser metal deposition was carried out on a polycrystalline substrate, epitaxial grain growth was attained when the substrate grains had a <100> crystallographic direction parallel to the local heat flow direction.

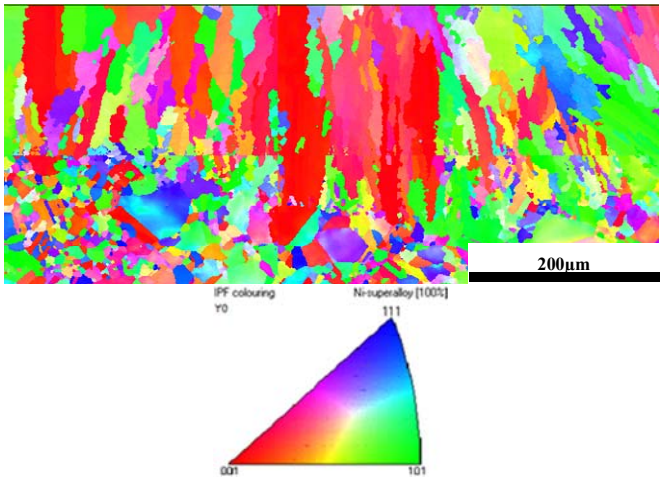

Fig. 8 The as-deposited Inconel 718 superalloy interface region using 950W (Orientated with build direction along the growth direction (Y))

Nucleation was favoured over growth in conditions at the CZ across the interface, where the PM had no grains with a <100> crystallographic orientation parallel to the heat flow direction. The grain morphology is mostly columnar with a common <100> crystallographic orientation which have grown rapidly, impeding the growth of other grains, this agrees strongly with Dinda et al.'s investigation [49]. Given the small overlap between adjacent tracks, most grains grew curved towards the heat source to attain maximum thermal gradient with proceeding growth like the dendritic morphology.

VI. Conclusion

A thermal model of the DED process for three process parameters of laser power, P = 550W, P = 750W and P = 950W was developed. An experimentally validated thermal model was implemented to predict the temperature history experienced during DED of IN718.

The interface region was diluted into four key aspects; CZ, PMZ, HAZ and PM with varying thermal histories, therefore varied microstructural response. The microstructure of the CZ was found to be non-uniform, consisting of columnar dendrites growing epitaxially along the build direction with interdendritic Laves phase. However, the PM microstructure was equiaxed with a uniform distribution of δ phase. The gaussian shape of the melt pool was indicative of dendrite growth towards maximum temperature. The dendrites were found to grow with respect to maximum thermal gradient, epitaxially from the substrate material. The PDAS decreased with decreasing laser power, therefore higher localized cooling rates were expected, given alterations to mechanical performance. During solidification of the LMD IN718, grains with the <100> crystallographic orientation grew epitaxially from the substrate and continued to grow into the deposit.

The thermal history captured by the simulation will be imperative to explain the microstructural response for the as-deposited interface region.

Acknowledgements

The authors would like to acknowledge the technical staff at the Advanced Forming Research Centre (AFRC) for their assistance with the laser metal deposition and we extended our thanks to the microscopy laboratory technicians of the AFRC for their support with the microstructure analyses.

References

[1] E. Hosseini and V. A. Popovich, "A review of mechanical properties of additively manufactured Inconel 718," *Addit. Manuf.*, vol. 30, no. September, p. 100877, 2019.

[2] L. J. Kumar and C. G. K. Nair, "Laser metal deposition repair applications for Inconel 718 alloy," in *Materials Today: Proceedings*, 2017, pp. 11068–11077.

[3] B. Graf, S. Ammer, A. Gumenyuk, and M. Rethmeier, "Design of experiments for laser metal deposition in maintenance, repair and overhaul applications," *Procedia CIRP*, vol. 11, pp. 245–248, 2013.

[4] S. Sreekanth, E. Ghassemali, K. Hurtig, and S. Joshi, "Effect of Direct Energy Deposition Process Parameters on Single-Track Deposits of Alloy 718," *Metals (Basel).*, vol. 10, no. 1, p. 96, 2020.

[5] P. Alvarez, M. Montealegre, J. Pulido-Jiménez, and J. Arrizubieta, "Analysis of the Process Parameter Influence in Laser Cladding of 316L Stainless Steel," *J. Manuf. Mater. Process.*, vol. 2, no. 3, p. 55, 2018.

[6] L. Costa, R. Vilar, T. Reti, and A. M. Deus, "Rapid tooling by laser powder deposition: Process simulation using finite element analysis," *Acta Mater.*, vol. 53, no. 14, pp. 3987–3999, Aug. 2005.

[7] H. Qi, M. Azer, and A. Ritter, "Studies of standard heat treatment effects on microstructure and mechanical properties of laser net shape manufactured INCONEL 718," *Metall. Mater. Trans. A Phys. Metall. Mater. Sci.*, vol. 40, no. 10, pp. 2410–2422, 2009.

[8] L. L. Parimi, R. G. A., D. Clark, and M. M. Attallah, "Microstructural and texture development in direct laser fabricated IN718," *Mater. Charact.*, vol. 89, pp. 102–111, Mar. 2014.

[9] E. L. Stevens, J. Toman, A. C. To, and M. Chmielus, "Variation of

hardness, microstructure, and Laves phase distribution in direct laser deposited alloy 718 cuboids," *Mater. Des.*, vol. 119, pp. 188–198, Apr. 2017.

[10] X. Zhao, J. Chen, X. Lin, and W. Huang, "Study on microstructure and mechanical properties of laser rapid forming Inconel 718," *Mater. Sci. Eng. A*, vol. 478, no. 1–2, pp. 119–124, Apr. 2008.

[11] M. Ma, Z. Wang, and X. Zeng, "Effect of energy input on microstructural evolution of direct laser fabricated IN718 alloy," *Mater. Charact.*, vol. 106, pp. 420–427, Aug. 2015.

[12] Q. Zhang, J. Yao, and J. Mazumder, "Laser Direct Metal Deposition Technology and Microstructure and Composition Segregation of Inconel 718 Superalloy," *J. Iron Steel Res. Int.*, vol. 18, no. 4, pp. 73–78, Apr. 2011.

[13] A. S. Johnson, S. Shao, N. Shamsaei, S. M. Thompson, and L. Bian, "Microstructure, Fatigue Behavior, and Failure Mechanisms of Direct Laser-Deposited Inconel 718," *Jom*, vol. 69, no. 3, pp. 597–603, 2017.

[14] S. Sui, J. Chen, R. Zhang, X. Ming, F. Liu, and X. Lin, "The tensile deformation behavior of laser repaired Inconel 718 with a non-uniform microstructure," *Mater. Sci. Eng. A*, vol. 688, pp. 480–487, Mar. 2017.

[15] R. G. Ding, Z. W. Huang, H. Y. Li, I. Mitchell, G. Baxter, and P. Bowen, "Electron microscopy study of direct laser deposited IN718," *Mater. Charact.*, vol. 106, pp. 324–337, 2015.

[16] L. J. Kumar and C. G. K. Nair, "Laser metal deposition repair applications for Inconel 718 alloy," *Mater. Today Proc.*, vol. 4, no. 10, pp. 11068–11077, Jan. 2017.

[17] E. Lertora, C. Mandolfino, and C. Gambaro, "Mechanical Behaviour of Inconel 718 Thin-Walled Laser Welded Components for Aircraft Engines," *Int. J. Aerosp. Eng.*, vol. 2014, pp. 1–9, 2014.

[18] W. J. Sames, K. A. Unocic, R. R. Dehoff, T. Lolla, and S. S. Babu, "Thermal effects on microstructural heterogeneity of Inconel 718 materials fabricated by electron beam melting," *J. Mater. Res.*, vol. 29, no. 17, pp. 1920–1930, 2014.

[19] E. R. Denlinger, J. C. Heigel, P. Michaleris, and T. A. Palmer, "Effect of inter-layer dwell time on distortion and residual stress in additive manufacturing of titanium and nickel alloys," *J. Mater. Process. Technol.*, vol. 215, pp. 123–131, 2015.

[20] J. C. Heigel, P. Michaleris, and E. W. Reutzel, "Thermo-mechanical model development and validation of directed energy deposition additive manufacturing of Ti–6Al–4V," *Addit. Manuf.*, vol. 5, pp. 9–19, Jan. 2015.

[21] P. Michaleris, "Modeling metal deposition in heat transfer analyses of additive manufacturing processes," *Finite Elem. Anal. Des.*, vol. 86, pp. 51–60, 2014.

[22] E. R. Denlinger and P. Michaleris, "Effect of stress relaxation on distortion in additive manufacturing process modeling," *Addit. Manuf.*, vol. 12, pp. 51–59, 2016.

[23] J. Ding *et al.*, "Thermo-mechanical analysis of Wire and Arc Additive Layer Manufacturing process on large multi-layer parts," *Comput. Mater. Sci.*, vol. 50, no. 12, pp. 3315–3322, 2011.

[24] T. R. Walker, C. J. Bennett, T. L. Lee, and A. T. Clare, "A validated analytical-numerical modelling strategy to predict residual stresses in single-track laser deposited IN718," *Int. J. Mech. Sci.*, vol. 151, pp. 609–621, Feb. 2019.

[25] S. M. Kelly, S. S. Babu, S. A. David, T. Zacharia, and S. L. Kampe, "A thermal and microstructure model for laser deposition of Ti-6Al-4V," in *Cost - Affordable Titanium*, 2004, pp. 45–52.

[26] M. Söderberg, A. Lundbaċk, and L. E. Lindgren, "Modeling of metal deposition," *Finite Elem. Anal. Des.*, vol. 47, pp. 1169–1177, 2011.

[27] R. G. Ding, Z. W. Huang, H. Y. Li, I. Mitchell, G. Baxter, and P. Bowen, "Electron microscopy study of direct laser deposited IN718," *Mater. Charact.*, vol. 106, pp. 324–337, 2015.

[28] D. Liu, J. C. Lippold, J. Li, S. R. Rohklin, J. Vollbrecht, and R. Grylls, "Laser engineered net shape (LENS) technology for the repair of Ni-base superalloy turbine components," *Metall. Mater. Trans. A Phys. Metall. Mater. Sci.*, vol. 45, no. 10, pp. 4454–4469, 2014.

[29] Z. Liu, H. Kim, W. Liu, W. Cong, Q. Jiang, and H. Zhang, "Influence of energy density on macro/micro structures and mechanical properties of as-deposited Inconel 718 parts fabricated by laser engineered net shaping," *J. Manuf. Process.*, vol. 42, pp. 96–105, Jun. 2019.

[30] S. M. Thompson, L. Bian, N. Shamsaei, and A. Yadollahi, "An overview of Direct Laser Deposition for additive manufacturing; Part I: Transport phenomena, modeling and diagnostics," *Addit. Manuf.*, vol. 8, pp. 36–62, Oct. 2015.

[31] E. R. Denlinger, V. Jagdale, G. V. Srinivasan, T. El-Wardany, and P. Michaleris, "Thermal modeling of Inconel 718 processed with powder bed fusion and experimental validation using in situ measurements," *Addit. Manuf.*, vol. 11, pp. 7–15, 2016.

[32] D. Dye, B. A. Roder, S. Tin, M. A. Rist, J. A. James, and M. R. Daymond, "Modeling and measurement of residual stresses in a forged IN718 superalloy disc," *Proc. Int. Symp. Superalloys*, pp. 315–322, 2004.

[33] A. P. Chakravarti, J. A. Goldak, and A. S. Rao, *Thermal Analysis of Welds.*, vol. 2. 1985.

[34] R. R. Unocic and J. N. DuPont, "Process Efficiency Measurements in the Laser Engineered Net Shaping Process," *Metall. Mater. Trans. B Process Metall. Mater. Process. Sci.*, vol. 35, no. 1, pp. 143–152, 2004.

[35] Y. Ono, T. Yuri, N. Nagashima, H. Sumiyoshi, T. Ogata, and N. Nagao, "High-cycle fatigue properties of Alloy718 base metal and electron beam welded joint," *Phys. Procedia*, vol. 67, pp. 1028–1035, 2015.

[36] W. Di Cao, "Solidification and solid state phase transformation of Allvac® 718Plus™ alloy," *Proc. Int. Symp. Superalloys Var. Deriv.*, pp. 165–177, 2005.

[37] Y. Zhang, Z. Li, P. Nie, and Y. Wu, "Effect of heat treatment on niobium segregation of laser-cladded IN718 alloy coating," *Metall. Mater. Trans. A Phys. Metall. Mater. Sci.*, vol. 44, no. 2, pp. 708–716, 2013.

[38] S. Azadian, L.-Y. Wei, and R. Warren, "Delta phase precipitation in Inconel 718," *Mater. Charact.*, vol. 53, no. 1, pp. 7–16, Sep. 2004.

[39] J. F. Radavich, "The Physical Metallurgy of Cast and Wrought Alloy 718," in *Superalloys 718 Metallurgy and Applications*, Vol. 1989., TMS, 1989, pp. 229–240.

[40] Y. Desvallees, M. Bouzidi, F. Bois, and N. Beaude, "Delta Phase in INCONEL 718: Mechanical Properties and Forging Process Requirements," pp. 281–291, 2012.

[41] Y. Zhang, L. Yang, T. Chen, W. Zhang, X. Huang, and J. Dai, "Investigation on the optimized heat treatment procedure for laser fabricated IN718 alloy," *Opt. Laser Technol.*, vol. 97, pp. 172–179, 2017.

[42] Y. Zhang, L. Yang, W. Lu, D. Wei, T. Meng, and S. Gao, "Microstructure and elevated temperature mechanical properties of IN718 alloy fabricated by laser metal deposition," *Mater. Sci. Eng. A*, vol. 771, no. October 2019, p. 138580, Jan. 2020.

[43] A. Segerstark, J. Andersson, L.-E. Svensson, and O. Ojo, "Microstructural characterization of laser metal powder deposited Alloy 718," *Mater. Charact.*, vol. 142, pp. 550–559, Aug. 2018.

[44] F. Liu *et al.*, "Microstructural changes in a laser solid forming Inconel 718 superalloy thin wall in the deposition direction," *Opt. Laser Technol.*, vol. 45, pp. 330–335, Feb. 2013.

[45] Y. Chen *et al.*, "Study on the element segregation and Laves phase formation in the laser metal deposited IN718 superalloy by flat top laser and gaussian distribution laser," *Mater. Sci. Eng. A*, vol. 754, pp. 339–347, Apr. 2019.

[46] S. Sui, J. Chen, X. Ming, S. Zhang, X. Lin, and W. Huang, "The failure mechanism of 50% laser additive manufactured Inconel 718 and the deformation behavior of Laves phases during a tensile process," *Int. J. Adv. Manuf. Technol.*, vol. 91, no. 5–8, pp. 2733–2740, Jul. 2017.

[47] F. Liu *et al.*, "The effect of laser scanning path on microstructures and mechanical properties of laser solid formed nickel-base superalloy Inconel 718," *J. Alloys Compd.*, vol. 509, no. 13, pp. 4505–4509, Mar. 2011.

[48] Y. Zhang, L. Yang, J. Dai, Z. Huang, and T. Meng, "Grain growth of Ni-based superalloy IN718 coating fabricated by pulsed laser deposition," *Opt. Laser Technol.*, vol. 80, pp. 220–226, 2016.

[49] G. P. Dinda, A. K. Dasgupta, and J. Mazumder, "Texture control during laser deposition of nickel-based superalloy," *Scr. Mater.*, vol. 67, no. 5, pp. 503–506, Sep. 2012.